The TRV Improvement of Fast Circuit Breakers Using Solid-State Series Superconducting Reactor

Heidary, Amir; Yazdani-Asrami, Mohammad; Hesami, Morteza; Sood, Vijay

DOI
10.1109/TPWRD.2022.3211778

Publication date
2022

Document Version
Final published version

Published in
IEEE Transactions on Power Delivery

The TRV Improvement of Fast Circuit Breakers Using Solid-State Series Superconducting Reactor

Amir Heidary, *Member, IEEE*, Mohammad Yazdani-Asrami, *Senior Member, IEEE*, Morteza Hesami, and Vijay Sood, *Life Fellow, IEEE*

***Abstract*—Utilizing superconducting technology in fault current limiters for power grid applications is a practical solution to achieve a more modern and efficient power system. This is due to their low-loss profile, high efficiency, and ability to transmit about 5x more power in the same footprint compared to conventional counterparts. In addition, the integration of renewable energy resources into power grids makes the use of fast circuit breakers essential. However, the Transient Recovery Voltage (TRV) of fast mechanical circuit breakers stays a concern. This paper studies the TRV of a fast circuit breaker during a fault condition. Then the effect of a solid-state superconducting series reactor (SSSR) on the TRV of the circuit breaker is investigated and compared using an analytical model, simulation studies, and experimental testing. The results prove that an SSSR significantly diminishes the TRV of the fast breaker and offers an effective superconducting solution for modern power grids.**

***Index Terms*—Fast circuit breaker, series reactor, superconductors, transient recovery voltage.**

I. Introduction

THE integration of distributed generation and renewable energy resources into modern grids is increasing the fault current level in the network, which affects the operation of mechanical fast circuit breakers (FCBs) [1]. The high Transient Recovery Voltage (TRV) of such breakers can damage the FCB and interrupt its effective performance during a fault in the network [2]. TRV is the voltage that appears across the circuit breaker terminals once the breaker interrupts a faulty line. TRV characteristics include a high rate-of-rise, a high-frequency oscillation depending on system *L-C* values, and a voltage magnitude higher than nominal system voltage, which can cause either a delayed or interrupted operation or even failure of the circuit breaker as well as its isolator [2]. Both fault level and TRV factors need to be met to prevent FCB failure based on IEEE Std C37.119-2016 [3].

The most common solution to protect FCBs from high fault current in the power network is to use either magnetic [4] or resistive [5], [6], [7] fault current limiters. Recently, superconducting fault current limiters (SFCLs) have also been recommended for such an application and present a promising new element of cryo-electrification for future modern power networks [8], [9], [10], [11]. Among diverse types of SFCLs, an inductive SFCL limits the fault current by inserting a large inductance in faulty lines [12], [13], whilst in the normal steady state, its inductance is exceptionally low [14], [15], [16]. The SFCL can be especially useful for protecting an FCB that is used primarily for limiting the fault current level [17], [18].

The other significant challenge for the operation of the FCB is the TRV across the FCB terminals. The TRV depends on the faulty system's equivalent resistance, inductance, and capacitance [19]. Moreover, the inductance of a faulty electric system with an uncontrolled inductive SFCL – i.e., affects TRV parameters such as the peak value of TRV, frequency, rate of rising recovery voltage (RRRV), and TRV damping constant [20].

This paper investigates the TRV of an FCB where a solid-state series superconducting reactor (SSSR) is employed as the TRV suppression system. By comparing the two scenarios (i.e., with and without an SSSR), it is shown that SSSR can effectively limit the magnitude of the TRV. In addition, it can also protect the FCB from a sharp RRRV, and its operation can be faster by reducing the TRV time constant.

The main achievements of this paper are:

- Improvement TRV of FCB using SSSR, and
- Reducing operational delay of FCB by decreasing the TRV time constant and magnitude of fault current

A. Analytical Study of TRV of FCB Without SSSR

In this section, the TRV of FCB is investigated, based on a simple electric system model illustrated in Fig. 1. In this 63 kV electric distribution system, the Thevenin model of an upstream grid is considered with an equivalent voltage source V_{th} and equivalent impedance Z_{th}. This is connected to the loads by an FCB and a short distribution line of impedance Z_{line}. It is assumed that a line-to-ground fault occurs at the end of the

Manuscript received 16 February 2022; revised 27 May 2022 and 9 August 2022; accepted 24 September 2022. Date of publication 10 October 2022; date of current version 24 March 2023. Paper no. TPWRD-00198-2022. *(Corresponding author: Amir Heidary.)*

Amir Heidary is with the IEPG Group, Department of Electrical Sustainable Energy Department, Delft University of Technology, 2628CD Delft, The Netherlands (e-mail: amir.powersys@gmail.com;a.heidary@tudelft.nl).

Mohammad Yazdani-Asrami is with the Propulsion, Electrification and Superconductivity group, James Watt School of Engineering, University of Glasgow, Glasgow G12 8QQ, U.K. (e-mail: m.yazdaniasrami@gmail.com).

Morteza Hesami is with the Department of Electrical Engineering, Zanjan Branch, Islamic Azad University, Zanjan 4515658145, Iran (e-mail: Morteza.hesami@iauz.ac.ir).

Vijay Sood is with the Department of Electrical, Computer and Software Engineering, Faculty of Engineering and Applied Science, Ontario Tech University, Oshawa, ON L1H 7K4, Canada (e-mail: vijay.sood@ontariotechu.ca).

Color versions of one or more figures in this article are available at https://doi.org/10.1109/TPWRD.2022.3211778.

Digital Object Identifier 10.1109/TPWRD.2022.3211778

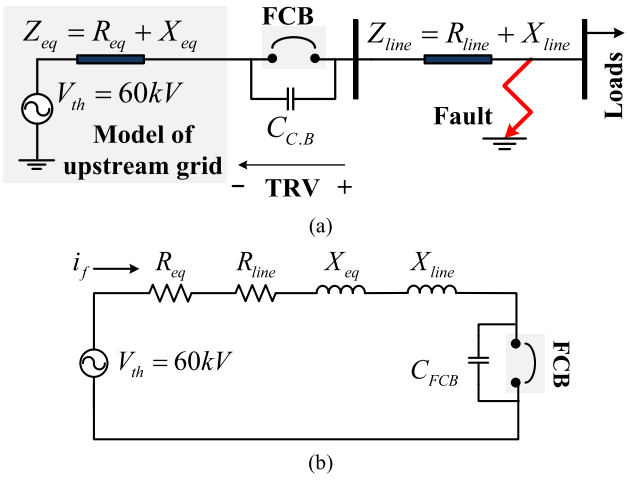

Fig. 1. a) Considered system model for analyzing TRV of FCB, b) simplified equivalent circuit model.

distribution line. The equivalent circuit of this electric system is shown in Fig. 1(b). In this case, the FCB operates to break the fault current, then the TRV of the FCB can be defined based on the circuit *R-L-C* parameters, as explained in IEEE C37.011-2011 [21].

As shown in Fig. 1(b), the simplified equivalent *R-L-C* circuit model is employed to analyze the TRV of FCB, where C_{FCB} is the shunt equivalent capacitance of the opened FCB. Kirchhoff's Voltage Law (KVL) for this system is written in (1), where the fault impedance is assumed to be negligible.

$$TRV = -v_{th}(t) + (R_{th} + R_{line})\,(i_f(t)) + (L_{th} + L_{line})\,\frac{di_f(t)}{dt} \tag{1}$$

$$\begin{cases} R_{eq} = R_{th} + R_{line} \\ L_{eq} = L_{th} + L_{line} \end{cases}$$

where, *TRV* is considered as the voltage of FCB; *t* refers to time and R_{th}, R_{line}, are the upstream grid Thevenin resistance and line resistance, respectively; and L_{th}, L_{line} are the upstream grid Thevenin inductance and line inductance, respectively. Also, i_f and v_{th} are the instantaneous current of the faulty line and upstream grid voltage, respectively.

The voltage of upstream grid $v_{th}(t)$ is defined as (2):

$$v_{th}(t) = V_m \cos \omega t \tag{2}$$

where V_m is the maximum voltage of upstream grid, *t* is the time and ω is the angular frequency of grid voltage.

The current in the faulty line is presented as:

$$i_f(t) = C_{FCB}\frac{d\,(TRV(t))}{dt} \tag{3}$$

By solving (1), TRV of FCB is obtained as (4) and then, its coefficients are given in (5).

$$TRV = -V_m\left(\frac{\omega_0^2 \cos \omega t}{\omega_0^2 - \omega^2} - \frac{\omega_0^2 k e^{-\alpha t}\cos \omega_0 t}{\omega_0^2 - \omega^2}\right) \tag{4}$$

TABLE I
SPECIFICATIONS OF THE ELECTRICAL SYSTEM

Electrical specification	Symbol	Value
Equivalent system resistance	R_{eq}	0.05 Ω
Source rms voltage	V_{th}	63 kV
Load impedance	Z_{Load}	600 + j60 Ω
Voltage source frequency	f_s	50 Hz
Equivalent system inductance	L_{eq}	5mH
Equivalent FCB capacitance	C_{FCB}	400 nF
Fault occurrence time	t_{fault}	0.42 s

$$\begin{cases} \omega_0 = 1/\sqrt{L_{eq}C_{C.B}} \\ \omega = 2\pi f \\ f_0 = \omega_0/2\pi \\ \alpha = R_{eq}/2L_{eq} \end{cases} \tag{5}$$

where ω_0 is the angular frequency of TRV oscillation, α is the damping coefficient, and *k* is a coefficient that depends on the initial voltage of the circuit, and it can vary between 1 and 2.

The peak magnitude of the TRV is obtained from (4), and its oscillation frequency strongly depends on the equivalent resistance and inductance values of the system. Moreover, the rate of rising recovery voltage (RRRV) is an important parameter for FCB operation, which is calculated from the peak magnitude of TRV and its oscillation frequency, as defined in IEC 62271-101 [22]. This is shown in (6), as follows:

$$RRRV = (\text{Max}\,(TRV))\,(2f_0) \tag{6}$$

B. Simulation of TRV of FCB Without SSSR

In this subsection, the TRV of FCB without SSSR is simulated in MATLAB-SIMULINK software. The specifications of the simulated system are provided in Table I.

Fig. 2 shows the simulation results for TRV of FCB without SSSR installed in the system when the fault occurred in t_{fault} = 0.42s. The peak TRV is 2.3 p.u., and its time constant is approximately 200 ms. After the TRV time constant is passed, its magnitude reaches the steady-state grid rms voltage value, i.e., equal to 63 kV which is considered the base voltage. In addition, as shown in the zoomed part in Fig. 2(b), the TRV frequency can be obtained in the time between 0.43-0.44 ms, which is approximately 3500 Hz. Thus, the RRRV of this case is calculated as 0.952 kV/us.

The TRV signal (Fig. 2) is in agreement with (4), where its time constant is correctly agreed by Napierian terms of (4) and its oscillation frequency $\omega_0/2\pi$ is given by the first part of the (5), and its RRRV is given by (6). These show the close agreement of simulation results with analytical equations. In addition, the current signal of the faulty line is depicted in Fig. 3, where the signal is zoomed upon interruption current once the FCB opens the faulty line.

It is shown that the system fault energy is dissipated over period of 200 ms. The first peak of fault current before FCB operation is 95 kA.

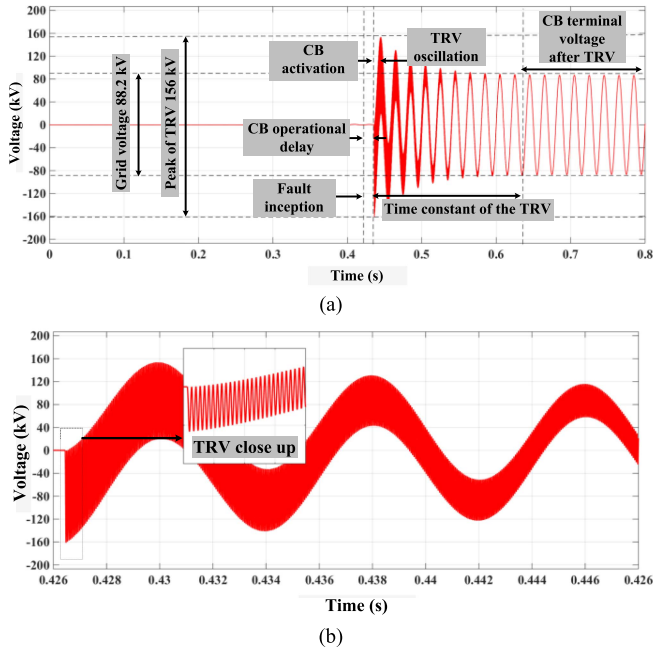

Fig. 2. a) TRV of FCB without using SSSR, b) TRV close-up view.

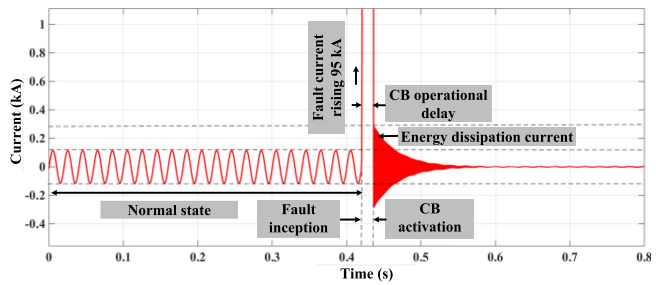

Fig. 3. line fault current without using SSSR.

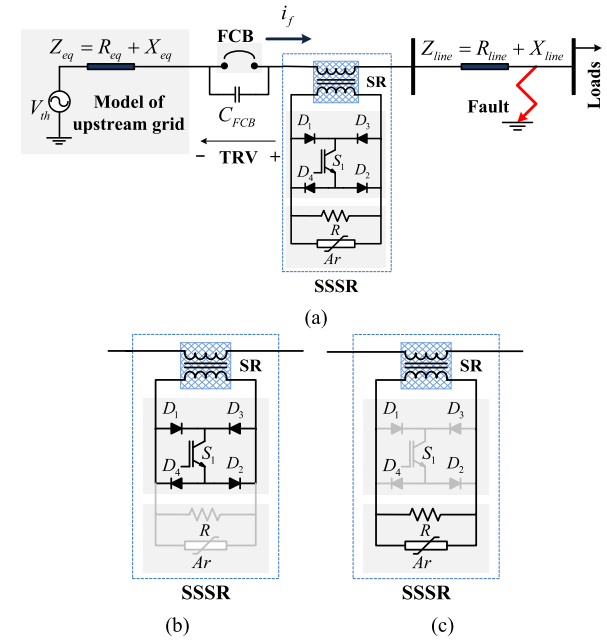

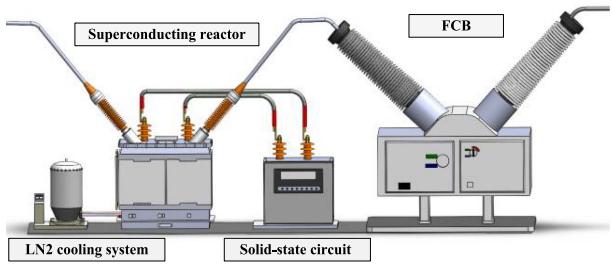

Fig. 4. SSSR structure and operation, a) SSSR Configuration, b) SSSR model in normal condition, c) SSSR model in fault condition. d) 3D scheme of SSSR configuration.

II. TRV OF FCB IN PRESENCE OF SSSR

In this section, first the configuration of the proposed SSSR and its operation principle/modes are discussed. Then, the structure of SSSR is mathematically modeled and analyzed. Finally, its operation is simulated in MATLAB-Simulink software.

A. Configuration and Operation Modes of SSSR

Fig. 4(a) illustrates the installed SSSR in series with the FCB in the system. The proposed SSSR structure comprises three main parts: a controllable superconducting reactor, a solid-state unit, and an energy-suppressing circuit. The series superconducting controlled reactor (SR) consists of a liquid nitrogen LN2 cooling system at saturation vapor pressure (SVP) 77 K [23], 50-meter superconducting Bi-2223 wire, and an EI ferromagnetic steel iron core. In the proposed SSSR, the voltage of the reactor's primary is two times less than the grid voltage, and the turns ratio of the reactor is 1:3, which shows that the secondary voltage is about 10 kV. The specifications of the SSSR, superconducting wire and the characteristics of the cooling system used in the simulation section are provided in Table II.

TABLE II
SPECIFICATIONS OF THE SSSR AND THE ELECTRICAL SYSTEM

Features	Description
SSSR specification:	
Wire material	Bi-2223
Stabilizer material	Cu alloy
Critical current	100 A/mm^2
Width	6 mm
Thickness	1.2 mm
Coolant	Liquid nitrogen LN2
Temperature	77 K
Electrical specification:	
SSSR provided inductance	100 mH
SSSR provided resistance	10 Ω

The solid-state unit comprises an IGBT switch S_1 and four diodes D_1-D_4. In the normal condition, as shown in Fig. 4(b), the IGBT is driven by a control pulse, and the diodes and IGBT conduct the current of the secondary winding of the SSSR. At the same time, the circuit breaker conducts electric power.

During the fault condition, as shown in Fig. 4(c), a protection trip signal is sent before FCB operation to SSSR, and then FCB

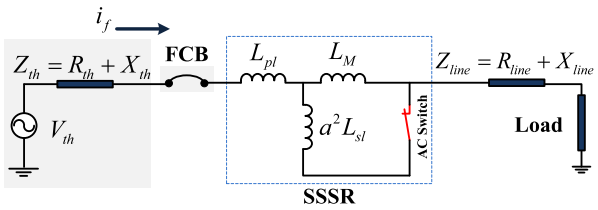

Fig. 5. SSSR model in the normal condition (IGBT S1 is ON) connected to the electric system and load.

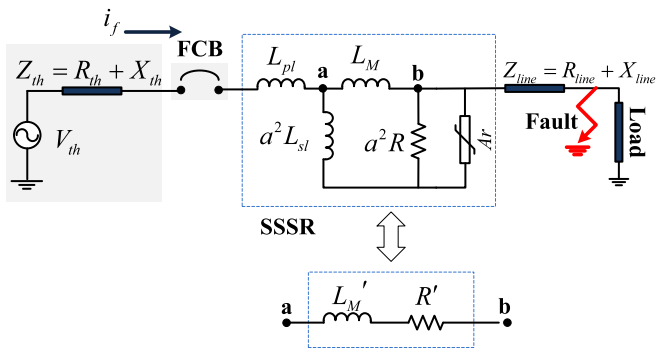

Fig. 6. The SSSR model under fault condition.

will operate. Therefore, the IGBT of the SSSR is turned-off once the FCB begins to break. At this time, resistance *R* and varistor *Ar* currents are drastically raised to effectively dampen out the system's stored energy and TRV of FCB.

Fig. 4(d) depicts a preliminary 3D installation design of the various parts of SSSR with a mechanical FCB.

Finally, the energy-suppressing circuit comprises a parallel resistor *R* and varistor *Ar*.

B. Analytical Study of SSSR

During the normal condition, the SSSR imposes its most negligible inductance on the system and transmits electric power from the upstream to the downstream grid. The IGBT and diodes perform this operation on the secondary side of the SR by conducting the secondary current with a negligible impedance. Fig. 5 shows the equivalent circuit of SSSR during normal conditions using a T-model of the applied reactor.

In Fig. 5, L_{pl} and L_{sl} are the SR's primary and secondary leakage inductances, respectively, and L_M is the magnetization inductance of the SR. In addition, a is the turns ratio of the SR primary and secondary coils (a is considered as N_p / N_s). By switching-on the IGBT S_1, the equivalent inductance of the SSSR is substantially reduced. (7) shows the line current under normal conditions.

$$I_{line} = \frac{V_{th}}{R_{th} + R_{line} + j\omega\left(L_{th} + L_{pl} + a^2 L_{sl} + L_{line}\right) + Z_{load}} \tag{7}$$

where, Z_{load} is the load impedance which is much higher than the small value of SSSR equivalent impedance.

During the fault condition, a fault trip command synchronously drives both the FCB and IGBT S_1.

As a result, FCB operates, the power line is open-circuited, and the IGBT S_1 is turned-off to suppress TRV of FCB to help with fast fault breaking. By opening the IGBT S_1, the current of the secondary side is commutated into the Arrestor (varistor) *Ar*, and damper Resistor *R*. In this operation, *Ar* protects the IGBT from peak voltage stress, and *R* damps the system transients. Fig. 6 shows the equivalent circuit of SSSR under the fault condition.

Under the fault condition, damper resistor *R* and varistor *Ar* are connected in parallel with the magnetization inductance L_M, and the inductances L_{pl} and L_{sl} can be effectively ignored. Under the fault condition, the TRV of FCB is given by (8).

$$TRV = V_{FCB} = -\frac{\frac{V_m}{\left(L_{eq}+L'_M\right)C_{FCB}}}{\frac{1}{\left(L_{eq}+L'_M\right)C_{FCB}} - (2\pi f)^2} \cdot \left(\cos(2\pi f t) - k e^{-\frac{R_{eq}+R'}{2\left(L_{eq}+L'_M\right)}t} \cos\left(\frac{t}{\left(L_{eq}+L'_M\right)C_{FCB}}\right)\right) \tag{8}$$

Considering (3), fault current i_f can be calculated by applying (8) in (3).

C. Proposed SSSR Power Loss Analysis

Total power loss of the SSSR consists of power loss of IGBTs and power loss of diode full bridges as follows:

$$P_{ss} = P_{IGBT} + P_{FB} \tag{9}$$

$$P_{IGBT} = n\left(V_{IGBT} I_s + R_{IGBT} I_s^2\right) \tag{10}$$

$$P_{FB} = (n/2)\, V_{Diode} I_s + \left(n R_{Diode} (I_s/2)^2\right) \tag{11}$$

where, P_{ss}, P_{IGBT}, and P_{FB} are power loss of solid-state units consisting of IGBTs and diodes power loss. I_s, V_{IGBT} and V_{Diode} are current of secondary, voltage drop of IGBTs and diodes. Moreover, n refers to the number of switches. In this analysis, the maximum possible voltage of reactor secondary is 18 kV, and the current in the normal state is roughly 300 A, considering that the turns ratio is 1:3. As a result, the maximum power loss of the SSSR is less than 10 kW, that is roughly 0.1% of system power flow.

D. Simulation Results of TRV of FCB Using SSSR

In Fig. 7, the TRV of FCB is shown when a fault occurs at 0.43 s. This figure shows that the magnitude of the TRV of FCB reaches 1.2 p.u., while the TRV time constant is limited to 20 ms which is in fair agreement with the Napierian (8), which proves to be an effective reduction of FCB operation delay. The obtained results show that the TRV frequency is effectively limited to 400 Hz in agreement with the first section of (5), and its RRRV is decreased to 0.065 kV/us, which is calculated by (6). The

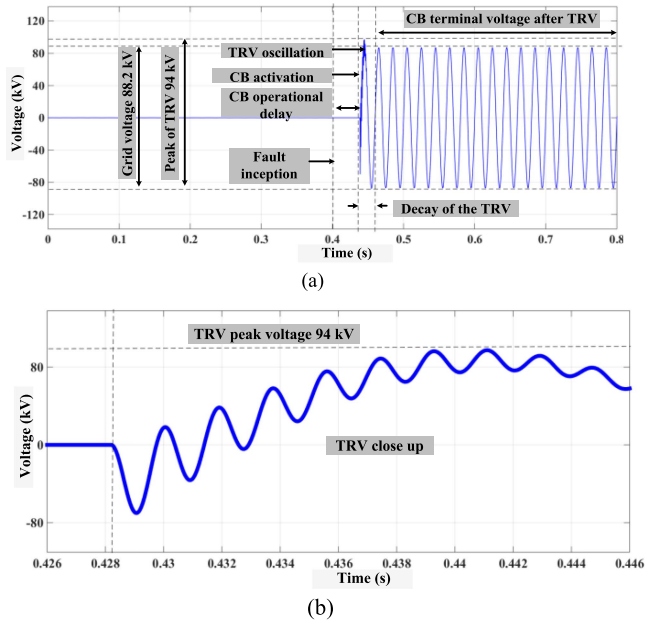

Fig. 7. a) TRV of FCB considering SSSR effect, b) close-up view of TRV.

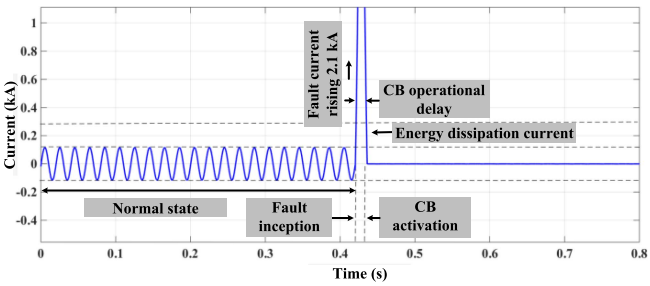

Fig. 8. a) line fault current considering SSSR effect.

simulation results prove the effectiveness of using the SSSR in the grid.

Furthermore, the current signal of a faulty line considering the effects of SSSR is depicted in Fig. 8. It is shown that the fault energy of the system is dissipated rapidly (in approximately 20 ms). The peak of fault current is 2.1 kA before the FCB operates.

III. Validation of the SSSR Magnetic Performance Using 3D Finite Elements Method

A. Analyzing SSSR Magnetic Equivalent Circuit

The physical model of the SSSR is presented in Fig. 9(a). using an E-I core. Its corresponding equivalent magnetic reluctance diagram is shown in Fig. 9(b).

The current in the primary winding of E-I core generates a magnetic flux φ_p. In contrast, the current in the secondary winding generates a flux φ_s in the opposite direction to the primary flux. Subtracting these two fluxes results in the main (central) arm core flux, known as the mutual flux.

Equation (12) calculates the series voltage drop of SSSR in the primary winding, which affects the TRV of FCB. This voltage

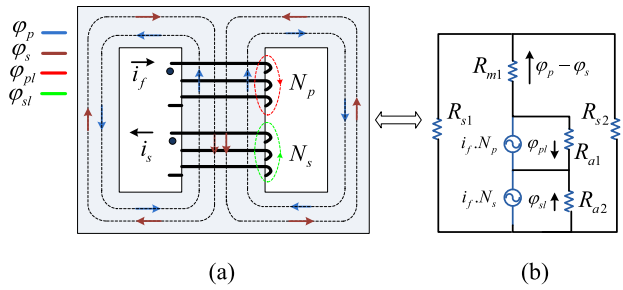

Fig. 9. a) Magnetic structure of SSSR b) electric equivalent circuit model.

is directly related to flux in the core, which, in the next stage, will be simulated by the finite element method (FEM) to validate SSSR operation during both normal and fault conditions.

$$V_{SSSR} = N_P^2 \left(\frac{di_f}{dt\,(R_{a1})} + \frac{(di_f - 0.3di_s)}{dt\left(\frac{R_m R_{s1} + R_m R_{s2} + R_{s1} R_{s2}}{R_{s1} + R_{s2}}\right)} \right) \tag{12}$$

where, i_f and i_s are currents of the primary and secondary windings, respectively. The number of turns in primary (N_p) is ten times smaller than secondary winding turns (N_s). φ_{pl} is the leakage flux of primary. In addition, R_m, R_{s1} and R_{s2} are the main and side arms' reluctances, respectively. Furthermore, R_{a1} is the leakage flux reluctance.

B. FEM Validation of SSSR

Due to the complex geometry and non-linear properties of most electromagnetic devices, FEM is usually employed for finding the magnetic field distribution and confirming the design structure. Numerical modeling is essential for the evaluation of the magnetic field distribution and the magnetization characteristic of the SSSR, which is inherently non-linear. Thus, in this section, the magnetic field distribution of the SSSR is decided using the 3D FEM with ANSYS-MAXWELL software. The geometric design of the proposed superconducting reactor is shown in Fig. 10.

Fig. 10(a) shows the coil's 2D and 3D views. A close-up of the 2D view shows that the SR coil is formed of a cryostat as a thermo-isolator that includes all the superconducting parts and coolant, primary and secondary windings, an electric paper sheet insulator, and separator cylindrical fiber insulation.

The SSSR core material is a magnetic steel iron that is designed with an EI-120 core structure, as illustrated in Fig. 10(b). It is also depicted in two 3D views of the SR, where the length-based meshes are applied in the 3D geometric model of the superconducting reactor.

In the first step of the FEM simulation, the magnetic field analysis of the core during normal operation is obtained; here, the secondary coil is bypassed by the AC switch, and the line current passes through the primary winding. Fig. 11(a) shows that the average flux density in the middle arm does not exceed 1.7 mT. The results from the FEM simulation confirm that, during normal operation, the imposed series inductance of SSSR is substantially low, resulting in a very low voltage drop.

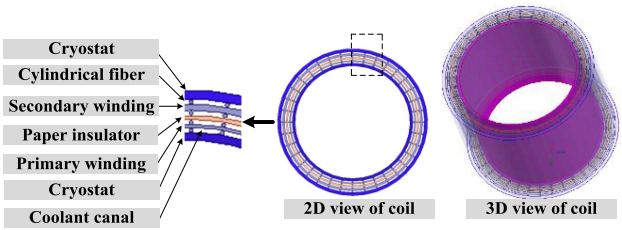

(a)

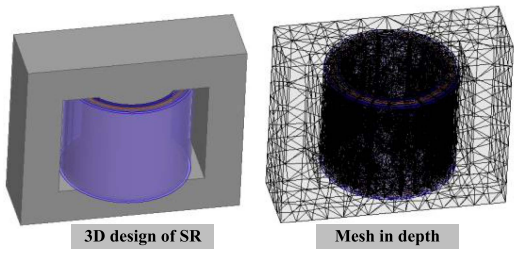

(b)

Fig. 10. a) Geometric view of SR coil, b) 3D design of SR and mesh sections.

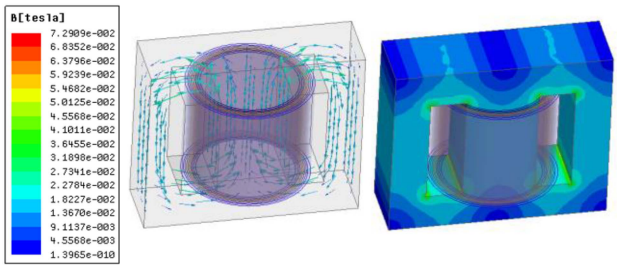

(a)

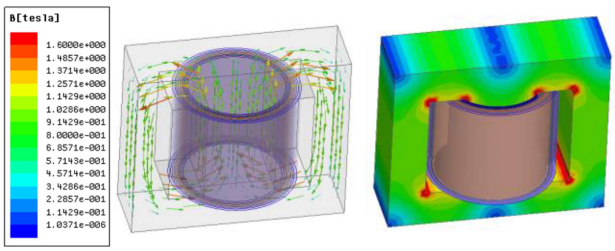

(b)

Fig. 11. a) Magnetic flux density of SR (normal condition), b) Magnetic flux density of SR (fault condition).

In the next step of the FEM simulation, the AC switch on the secondary side is opened. The commutation of current limits the current in the secondary winding into the damper resistor *R*. Fig. 11(b) shows that the average magnetic flux density of the main arm reaches 1.1 T at its maximum value. In contrast, the magnetic flux density in the saturation state was 1.8 T. The simulation results confirm that the SSSR can impose considerable inductance and resistance to suppress the TRV of the FCB to an acceptable level. It is also noteworthy that the flux density in the corners of the core is much higher than in other directions, but it doesn't reach the saturation level.

TABLE III
SPECIFICATIONS OF TEST SETUP

Features	Description
Core size	EI-120
Switch type	IGBT, HGTP10N50C1
Diode type	Metal packaged, 5A, 400 V
Source voltage	350 V
Load impedance	25 + j10 Ω

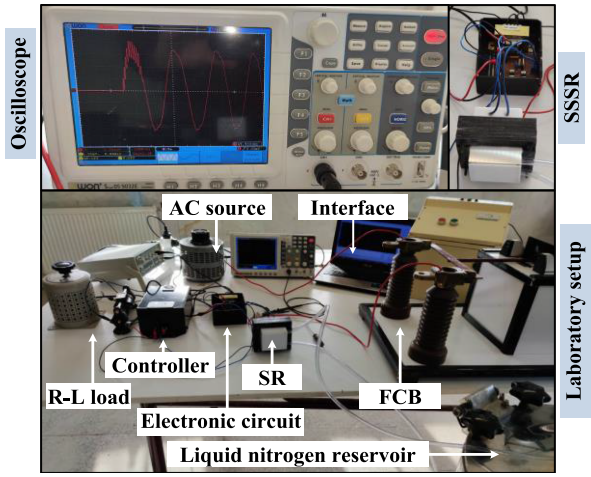

Fig. 12. Experimental setup for evaluating the proposed SSSR prototype.

IV. EXPERIMENTAL VALIDATION OF THE SSSR PERFORMANCE

In this section, the experimental setup is used to compare the TRVs of the FCB with and without SSSR. This experimental test confirms the operation of SSSR. The specifications of the test setup are provided in Tables II and III.

Fig. 12 shows the experimental setup of the SSSR. This setup is based on the simulated test model shown in Fig. 4. The scaled-down prototype is fed from a 350 V AC source, considered as base voltage.

A low-voltage fast mechanical breaker is employed to examine its TRV. In this laboratory setup, a fault is started by a controller at the same adjusted time. The same controller also generates the trip command.

To build the SSSR prototype, an EI-120 ferromagnetic core is used. The cryostat package is also based on this core size. Next, the superconducting windings (primary and secondary) are wound around the core, placed in the cryostat, and liquid nitrogen is injected into the superconducting coil. Finally, the primary winding of the SSSR is connected in series with FCB, and the secondary winding is connected to the electronic circuit. The electronic circuit includes an IGBT switch, four full-bridge diodes, a 20 Ω, 5 W resistor, 500 V varistor, and a controller.

A. FCB TRV Measurement Without SSSR

In the first experimental test, the TRV of FCB is measured considering that there is no installed SSSR in series with the FCB. The measured TRV signal, shown in Fig. 13(a), reaches a peak value of 1.8 p.u. In addition, it experiences a relatively

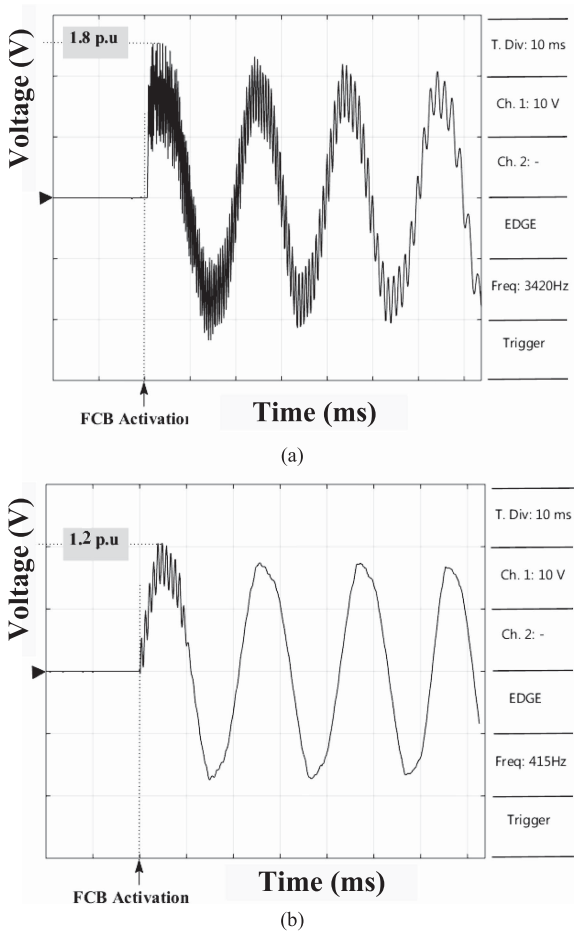

Fig. 13. Measured signal of TRV of FCB (probe X25), a) without SSSR installation b) with SSSR operation.

high RRRV of 0.0044 kV/us, which is in close agreement with (6). Its frequency is slightly higher than 3.4 kHz, which agrees with (5). Its time constant is approximately 200 ms, which is confirmed by the Napierian function of (4).

B. FCB TRV Measurement With SSSR

In the second experimental test, the SSSR is connected in series with the mechanical FCB to suppress its TRV. The controller causes a fault at the same time as the first test, and the FCB is activated to interrupt the fault current and use the SSSR to suppress the TRV of the FCB. Considering Fig. 13(b), the peak value of TRV now reaches 1.2 p.u., which is about 33% less than the earlier test without the SSSR.

Additionally, the TRV frequency is 415 Hz, in good agreement with (5), and its RRRV is reduced to 0.0004 kV/us, which agrees with (6). Its time constant is approximately 20 ms which proves the reduction of the FCB operation delay that is confirmed by the Napierian function of (8). This test supports the results obtained previously from both analytical and simulation studies.

To show the performance of the SSSR, a more profound comparison of the simulation and experimental tests is provided in Table IV, where TRV peak value, RRRV, TRV damping

TABLE IV
TRV OF FCB: EXPERIMENTAL AND SIMULATION RESULTS

Compared data	Simulation results		Experimental results	
	With SSSR	Without SSSR	With SSSR	Without SSSR
TRV peak (p.u.)	1.2	2.3	1.2	1.8
RRRV (kV/us)	0.065	0.952	0.0004	0.0044
Duration (ms)	20	200	20	200
Frequency (Hz)	400	3500	415	3420
Fault current peak (kA)	2.1	95	0.0045	0.215

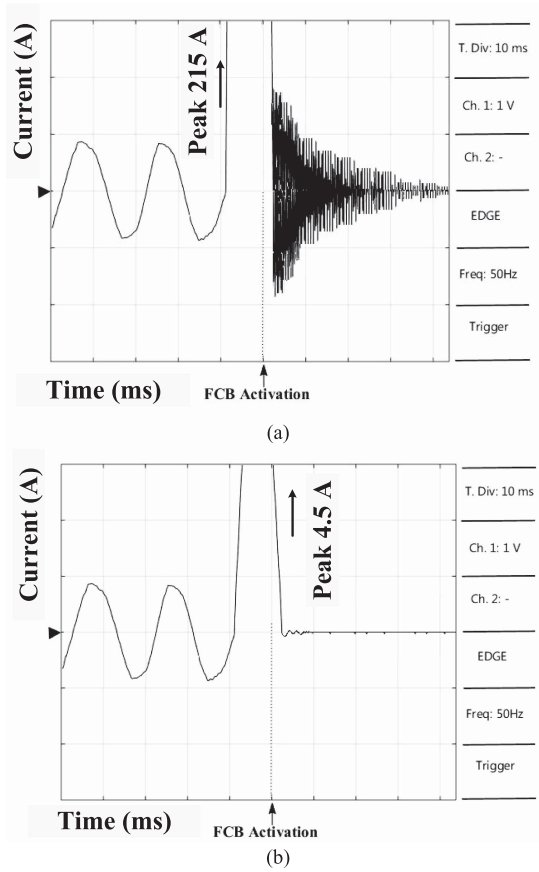

Fig. 14. Measured signal of fault current (probe X25), a) without SSSR installation b) with SSSR operation.

duration, and TRV frequency are given. Considering the SSSR effect, it is noted that the TRV peak reduces by about 33%, damping duration reduces by about 80%, frequency reduces by about 90%, and RRRV reduces by about 91%.

In Fig. 14(a), it is illustrated that the peak magnitude of fault current reaches 215 A. After FCB operation, fault current interrupts after roughly 200 ms. On the other hand, by installing the SSSR, the peak of fault current reduces to 4.5 A, and then, by operation of FCB, it is interrupted within 20 ms, as depicted in Fig. 14(b).

Based on the test and implementation of the scale down prototype, the possibility of implementation of grid-scale SSSR is concluded where the maximum voltage drop of SSSR is less than grid voltage and its resistance is almost zero because of its superconducting structure.

So, from both isolation design and power loss point of view, the proposed structure will be economic. In addition, designing an LN2 cooling system for a small-size series reactor (100 mH, 100 A) is reasonably economic. Furthermore, the design of the 10 kV IGBT package (in the secondary section) is mature and economic, based on commercially available power electronic equipment in the market.

V. Conclusion

In this paper, the feasibility design of a solid-state series superconducting reactor (SSSR) is presented. It is utilized to suppress transient recovery voltage (TRV) of mechanical fast circuit breakers (FCBs), which are used to protect the FCB and reduce its operational delay, besides fault current limitation of faulty line. The proposed SSSR consists of a controllable superconducting reactor, four diodes and an IGBT as a solid-state unit, and a parallel resistor and arrester combination as the energy-suppressing circuit. The experimental test results agreed with the simulation findings and confirmed the effectiveness of installing the SSSR in a sample distribution network to suppress the TRV of FCB and limit the fault current. It is concluded that by installing the SSSR, the peak TRV, damping duration, frequency, and RRRV of FCB were reduced by about 33%, 80%, 90%, and 91%, respectively. Moreover, the magnitude of fault current declined to around 97%. Therefore, a lower rating of FCB can be utilized. Accordingly, SSSR mainly affects future modern grids to use more economic surge arresters and circuit breakers. It is worth noting that SSSR is not aimed at replacing surge arresters at this stage. However, it can help to use lower rating surge arresters, and it will offer other limiting features to make the grip more reliable and safer. Future work would entail designing a compact, high-performance circuit breaker with the ability to operate faster than existing AC breakers, including both fault current limiter and TRV-suppressing structures. In addition, a follow-up to the research investigated in this paper can be considering multiple reclosures into a fault by the duty cycle of the FCB and considering the energy and heat dissipated during fault and their influence on the FCB and on SSSR itself.

References

[1] H. Radmanesh, S. H. Fathi, G. B. Gharehpetian, and A. Heidary, "A novel solid-state fault current-limiting circuit breaker for medium-voltage network applications," *IEEE Trans. Power Del.*, vol. 31, no. 1, pp. 236–244, Feb. 2016.

[2] R. Rifaat, T. S. Lally, and J. Hong, "Circuit breaker transient recovery voltage requirements for medium-voltage systems with NRG," *IEEE Trans. Ind. Appl.*, vol. 50, no. 5, pp. 2989–2995, Sep./Oct. 2014.

[3] IEEE Guide for Breaker Failure Protection of Power Circuit Breakers, IEEE Std C37.119-2016 (Revision of IEEE Std C37.119-2005), pp. 1–73, Jul. 2016.

[4] A. Heidary, H. Radmanesh, K. Rouzbehi, A. Mehrizi-Sani, and G. B. Gharehpetian, "Inductive fault current limiters: A review," *Elect. Power Syst. Res.*, vol. 187, Oct. 2020, Art. no. 106499.

[5] M. Noe, A. Hobl, P. Tixador, L. Martini, and B. Dutoit, "Conceptual design of a 24 kV, 1 kA resistive superconducting fault current limiter," *IEEE Trans. Appl. Supercond.*, vol. 22, no. 3, Jun. 2012, Art. no. 5600304.

[6] W. Song, X. Pei, J. Xi, and X. Zeng, "A novel helical superconducting fault current limiter for electric propulsion aircraft," *IEEE Trans. Transp. Electrific.*, vol. 7, no. 1, pp. 276–286, Mar. 2021.

[7] B. Xiang, L. Gao, Z. Liu, Y. Geng, and J. Wang, "Short-circuit fault current-limiting characteristics of a resistive-type superconducting fault current limiter in DC grids," *Supercond. Sci. Technol.*, vol. 33, no. 2, 2020, Art. no. 024005.

[8] J. Xi, X. Pei, W. Song, B. Xiang, Z. Liu, and X. Zeng, "Experimental tests of DC SFCL under low impedance and high impedance fault conditions," *IEEE Trans. Appl. Supercond.*, vol. 31, no. 5, Aug. 2021, Art. no. 5601205.

[9] H. Li et al., "Effect of arc chute on DC current interruption by liquid nitrogen in HTS electrical system of distributed propulsion aircraft," *IEEE Trans. Appl. Supercond.*, vol. 31, no. 5, Aug. 2021, Art. no. 5601305.

[10] W. Song et al., "Experimental and simulation study of resistive helical HTS fault current limiters: Quench and recovery characteristics," *IEEE Trans. Appl. Supercond.*, vol. 31, no. 5, Aug. 2021, Art. no. 5601106.

[11] W. Song et al., "AC losses in noninductive SFCL solenoidal coils wound by parallel conductors," *IEEE Trans. Appl. Supercond.*, vol. 30, no. 8, Dec. 2020, Art. no. 5602509.

[12] M. Majka, J. Kozak, S. Kozak, G. Wojtasiewicz, and T. Janowski, "Design and numerical analysis of the 15 kV class coreless inductive type SFCL," *IEEE Trans. Appl. Supercond.*, vol. 25, no. 3, Jun. 2015, Art. no. 5601005.

[13] J. Kozak, M. Majka, S. Kozak, and T. Janowski, "Comparison of inductive and resistive SFCL," *IEEE Trans. Appl. Supercond.*, vol. 23, no. 3, Jun. 2013, Art. no. 5600604.

[14] H. Kado, M. Ichikawa, M. Shibuya, M. Kojima, M. Kawahara, and T. Matsumura, "Inductive type fault current limiter using bi-2223 thick film on MgO cylinder with bi-2212 buffer layer," *IEEE Trans. Appl. Supercond.*, vol. 15, no. 2, pp. 2051–2054, Jun. 2005.

[15] A. Heidary, H. Radmanesh, K. Rouzbehi, and H. M. CheshmehBeigi, "A multifunction high-temperature superconductive power flow controller and fault current limiter," *IEEE Trans. Appl. Supercond.*, vol. 30, no. 5, Aug. 2020, Art. no. 5601208.

[16] A. Heidary, H. Radmanesh, K. Rouzbehi, and J. Pou, "A DC-reactor-based solid-state fault current limiter for HVdc applications," *IEEE Trans. Power Del.*, vol. 34, no. 2, pp. 720–728, Apr. 2019.

[17] M. R. Barzegar and M. Niasati, "Fusion TRV limiter a solution to modify interrupting characteristics of CBs with presence of resonance type SFCL," in *Proc. IEEE 30th Int. Power System Conf.*, 2015, pp. 92–98.

[18] A. Heidary, K. Rouzbehi, A. Mehrizi-Sani, and V. K. Sood, "A self-activated fault current limiter for distribution network protection," *IEEE J. Emerg. Sel. Topics Power Electron.*, vol. 10, no. 4, pp. 4626–4633, Aug. 2022, doi: 10.1109/JESTPE.2021.3109217.

[19] D. Huang, S. Shu, and J. Ruan, "Transient recovery voltage distribution ratio and voltage sharing measure of Double- and Triple-Break vacuum circuit breakers," *IEEE Trans. Compon., Packag. Manuf. Technol.*, vol. 6, no. 4, pp. 545–552, Apr. 2016.

[20] X. Cheng, Z. Chen, G. Ge, Y. Wang, M. Liao, and L. Jiao, "Dynamic dielectric recovery synergy of hybrid circuit breaker with CO2 gas and vacuum interrupters in series," *IEEE Trans. Plasma Sci.*, vol. 45, no. 10, pp. 2885–2892, Oct. 2017.

[21] IEEE Guide for the Application of Transient Recovery Voltage for AC High-Voltage Circuit Breakers with Rated Maximum Voltage above 1000 V, IEEE Standard C37.011-2011 (Revision of IEEE Standard C37.011-2005), pp. 1–127, May 2019.

[22] High-voltage switchgear and control gear - Part 101: Synthetic testing, IEC 62271-101 2021.

[23] K. Funaki et al., "Development of low-AC-loss bi-2223 superconducting multifilamentary wires," *IEEE Trans. Appl. Supercond.*, vol. 19, no. 3, pp. 3053–3056, Jun. 2009.